Geotech Geol Eng
https://doi.org/10.1007/s10706-024-02927-w

ORIGINAL PAPER

Numerical Investigation of Load Transfer in Geosynthetic-Reinforced Embankments Over Cavities: Effects of Opening Process and Cyclic Loading

Minh-Tuan Pham · Duc-Duy Nguyen · Tung-Duong Nguyen · Van-Hung Pham

Received: 7 March 2024 / Accepted: 27 August 2024

Abstract During the construction of urban roads and infrastructure, factors such as groundwater, soil subsidence, and underground erosion can lead to the formation of cavities. Using geosynthetics to reinforce embankments over these cavities has demonstrated technical and economic efficiency while reducing construction time. Previous studies have explored stress transfer processes, including the arching effect within embankments, the membrane effect of geosynthetics, and settlement of the embankment and ground. However, these studies have been limited in their examination of cavity-opening processes. This paper uses the finite element method to analyze load transfer in geosynthetic-reinforced embankments over cavities, considering cavity opening processes and the effect of cyclic loading. The numerical model is built based on the experimental work of Villard and Briançon (Can Geotech J 45: 196–209, 2008). The numerical results are validated against experimental results, confirming the reliability of the numerical modeling. The results also show that the gradual expansion of the cavities leads to an increase in surface deformation, geosynthetic deflection, and the formation of a conical stress distribution pattern. Increasing the number of cyclic loads induces a reduction in stress transfer within the embankment while increasing surface settlement and geosynthetic deflection. Additionally, a mathematical equation for the distribution of stress acting on the geosynthetic is proposed to enhance the accuracy of previous analytical methods.

Keywords FEM · Geosynthetics · Soil arching · Cavity · Cyclic loading · Opening process

M.-T. Pham (✉)
Department of Geotechnical Engineering, Faculty of Geology and Petroleum Engineering, Ho Chi Minh City University of Technology (HCMUT), 268 Ly Thuong Kiet Street, District 10, Ho Chi Minh City, Vietnam
e-mail: pmtuan@hcmut.edu.vn

M.-T. Pham
Vietnam National University Ho Chi Minh City (VNU-HCM), Linh Trung Ward, Thu Duc City, Ho Chi Minh City, Vietnam

D.-D. Nguyen · T.-D. Nguyen
Laboratory of Geotechnics, Faculty of Geology and Petroleum Engineering, Ho Chi Minh City University of Technology (HCMUT), 268 Ly Thuong Kiet Street, District 10, Ho Chi Minh City, Vietnam
e-mail: ducduyentus@gmail.com

T.-D. Nguyen
e-mail: ntduong.sdh241@hcmut.edu.vn

V.-H. Pham
Department of Infrastructure Engineering, Faculty of Civil Engineering, Hanoi University of Mining and Geology (HUMG), 18 Vien Street, North Tu Liem District, Hanoi City, Vietnam
e-mail: phamvanhung@humg.edu.vn

List of Symbols

2D	Two-dimensional
c	Cohesion (kN/m^2)
B	Cavity width (m)

Published online: 30 August 2024

D	Downward opening
DEM	Discrete element method
E	Efficacy of load transfer (%)
E'	Young's modulus (kN/m^2)
FEM	Finite element method
GSY	Geosynthetic reinforcement
H	Embankment height (m)
J	Geosynthetic stiffness (kN/m)
L	Length of foundation soil (m)
L_L	Length of left side of cavity (m)
L_R	Length of right side of cavity (m)
N	Number of load cycle
P	Progressive opening
q	Top load (kPa)
Q	Load applied on the geosynthetic situated above cavity (kPa)
φ	Friction angle (°)
ψ	Dilatancy angle of filling soil (°)
ν	Poisson ratio
γ	Unit weight (kN/m^3)

1 Introduction

The presence of cavities or sinkholes causes surface settlements and foundation damage, posing a high risk to the durability and stability of constructions. Cavities typically form due to human activities including underground construction (Singh and Dhar 1997) and groundwater exploitation, and natural processes such as tectonic activity, washout, and weathered phenomena (Gutiérrez et al. 2008; Serridge and Cooper 2023). It is challenging for engineers to determine the location and the probability of its occurrence (El Ganainy et al. 2016; Brahmi et al. 2023). When a cavity is detected, investigation, cause analysis, and development forecasting must be conducted. Subsequent treatment solutions are proposed to prevent cavity enlargement and reinforce the cavity top. This creates challenges in meeting technical requirements, extends processing times, increases costs, and may render the associated work unusable. Therefore, reinforcing the embankment to minimize the formation of cavities is considered a safe solution, reducing costs and not affecting the exploitation and operation of the construction.

Geosynthetics are synthetic materials characterized by high strength and low strain. It has been frequently employed for soil reinforcement. The solution of the geosynthetic reinforced embankment restricts the formation of localized cavities (Giroud et al. 1990; Villard et al. 2000; Blivet et al. 2002; Van Dyk and Jacobsz 2016). This method offers various advantages including simplicity, easy installation, and cost-effectiveness. Research has been conducted to clarify the load transfer mechanism and settlement of an embankment above a cavity subjected to static load (Wang et al. 1996). Under the weight and applied loads, the soil-geosynthetic system induces two primary effects: bending of the soil layer and stretching of the geosynthetic reinforcement. The soil layer bending sets up the soil arching, which transmits a portion of the applied load away from the void zone. The geosynthetic stretching forms a part of the strength of the geosynthetic due to the 'tensioned membrane'. The tensioned membrane theory was first proposed by Giroud (1981) to evaluate the bridging load of a geosynthetic over a void. Subsequently, a design chart was developed based on tensioned membrane theory. The chart has been used to define the load capacity of geosynthetics. Bonaparte and Berg (1987) have suggested that using the combination of arching and tensioned membrane theories enables the design approach more realistic. This way was further developed by Giroud et al. (1988, 1990) for the investigation and design of a geosynthetic reinforced embankment over a void.

Previous researchers (Gabr and Hunter 1994; Briançon and Villard 2008; Huckert et al. 2016; Pham et al. 2018a, 2022; Villard et al. 2016; Chalak et al. 2019; Pham 2019) have identified that the expansion of filling material and the load transfer within the embankment are the primary complex mechanisms in a geosynthetic-reinforced embankment over cavities. The expansion coefficient is defined as the ratio between the final volume of the collapsed soil mass within the embankment above the cavity and its initial volume. The coefficient of expansion (Ce) of embankment fill characterizes the change in the volume of the deformation zone within the embankment, playing a crucial role in connecting geosynthetic deflection and surface settlement of the embankment. In existing design methods such as BS8006 (2010), RAFAEL (Blivet et al. 2002; Villard et al. 2000), and EBGEO (2010), geosynthetic deflection is initially assumed. Due to Ce, surface settlement is estimated. Thus, given the critical role of Ce, it is important to determine the precise volume of the deformation

zone within the embankment fill, which is determined from the shapes of the settlement surface and geosynthetic deflection. The geosynthetic deflection and the surface settlement have a critical relationship in estimating the maximum deformation above the cavities. There are various methods to estimate the shapes of geosynthetic deflection and surface settlement. In existing design methods such as BS8006 (2010), RAFAEL (Blivet et al. 2002; Villard et al. 2000), and EBGEO (2010), the shapes of geosynthetic deflection and surface settlement were assumed as a parabolic curve. However, the experimental results of Pham et al. (2018a) and Silva and Elshafie (2021a) suggested that a third-order polynomial function more accurately fits the geosynthetic deflection shape and the surface settlement.

The efficacy of load transfer within geosynthetic-reinforced embankments has been evaluated by many authors (Terzaghi 1943; Hewlett and Randolph 1988; Girout et al. 2014; Pham and Dias 2021a; Rui et al. 2022) using the efficacy coefficient, denoted by E. For a reinforced embankment over cavities, the efficacy coefficient is calculated using Eq. (1), similar to the function proposed by Villard et al. (2016). This coefficient depends on the difference between the applied load on the cavity area before and after the opening, with values ranging from 0 to 100%.

$$E(\%) = \frac{W_i - Q_g}{W_i} \tag{1}$$

where E is the efficacy, W_i is the total load acting on the cavity (kN), including the weight of embankment material situated over the cavity area and surcharge placed above before cavity opening (kN), and Q_g is the applied load on the geosynthetic above the cavity after the opening (kN).

Besides investigating the behavior of reinforced embankment over a cavity, the influences of various parameters such as the surcharge, the model's geometrical features, the filling material, and particularly the cavity opening method have been studied (Agaiby and Jones 1996; Huckert et al. 2016; Villard et al. 2016; Pham et al. 2022). Most previous research analyzed the influence of parameters on the load transfer mechanism, the surface settlement, and geosynthetic deflection. The analyses indicated that the embankment thickness with the geosynthetic is a significant parameter for the load transfer. The critical height of the embankment, denoted as H_c, is another crucial parameter influencing the load distribution. It represents the threshold value of embankment height at which the full degree of soil arching is achieved. When the height of the embankment reaches the critical value or in other words, the cavity appears at a sufficiently deep position, the differential settlement between the subsided area and the remaining area can be neglected. This can be explained by the fact that when the distance between the cavity and the surface is large enough, shear stress is mobilized in the embankment, allowing the weight of the fill above the cavity to be transferred by the arching effect. A wide range of ratios between the critical height of embankment and cavity width, H_c/B has been reported in the relevant studies of Potts and Zdravkovic (2010); Villard et al. (2016); and Silva and Elshafie (2021b) with values ranging from 0.25 to 2.0.

The friction angle of the fill soil had a minor influence on surface settlement (Briançon and Villard 2008). In addition, the softer the fill material is, the greater the surface settlement is, and the smaller the degree of arching is. The effect of the geosynthetic properties on the load transfer was not as important as the cavity diameter and the soil properties (Agaiby and Jones 1996). An increase in the surcharge load induced a negligible change in the efficacy, which varied from 52 to 56%. Both the surface deformation and the geosynthetic deflection developed when the surcharge load increased (Pham et al. 2022).

Regarding the influence of the cavity opening process, laboratory experiments and numerical modeling of Huckert et al. (2016) and Villard et al. (2016) have been conducted for cavities with varying sinkhole diameters. The influence of the width of the cavity on the load transfer, geosynthetic deflection, and surface settlement were made clear. Huckert et al. (2016) conducted full-scale experimental tests to study the mechanisms of load transfer within geosynthetic reinforced embankments over various voids. The experimental results figured out the influence of fill material on the surface settlement, the tensile strength, and the shape of deflected geosynthetic. In the case of granular material, as the opening process widened, surface deformation progressively increased until collapse, during which the tensile strength of the geosynthetic increased, and the geosynthetic deflection exhibited a parabolic shape. Meanwhile, in the cohesive treated soil case, the surface settlement was insignificant, and

the soil collapsed as the surcharge was increasingly applied. The falling soil induced a horizontal shape of the geosynthetic at the cavity center, which reflected the non-uniform stress on the geosynthetic. Based on the experimental investigation of Huckert et al. (2016), Villard et al. (2016) conducted a numerical analysis of the geosynthetic-reinforced embankments overlying voids. The numerical outcomes demonstrated that the cavity opening procedure had a significant impact on the stress distribution in the geosynthetic reinforcement above the cavity and influenced the soil deformation mechanism. Furthermore, the soil expansion coefficient was not a constant within the embankment, it was strongly dependent on the cavity formation process.

In the literature, the influence of cyclic loading on the load transfer mechanism within a geosynthetic-reinforced embankment has been considered by the experimental and numerical studies (Han et al. 2011, 2015; Benmebarek et al. 2015; Houda et al. 2016, 2019; Pham et al. 2018b; Pham and Dias 2021b). The studies showed that cyclic loading caused a decrease in the degree of soil arching and the cumulated settlements. In fact, a certain number of loading cycles might limit the arching effect. Zhuang and Li (2015) carried out 3D numerical analyses to investigate a geosynthetic-reinforced embankment under cyclic loading, in which the Mohr–Coulomb model for embankment used and demonstrated a significant impact on the embankment settlement due to cyclic loads. However, most of these studies were developed with the problem of the embankments on rigid pile-reinforced soft soil, either with or without the presence of geosynthetics. In terms of the behavior of a geosynthetic reinforced embankment above a cavity subjected to cyclic loading, there have not been many conducted studies. Huckert et al. (2016) carried out the experimental model subjected to 10 load cycles. The final displacement values were stable after the 1st loading cycle.

While achieving notable results, it is clear that the impacts of both cavity opening methods and cyclic loadings have not been thoroughly assessed. To address this gap, this paper investigates the opening process and cyclic loading on the performance of a geosynthetic-reinforced embankment over cavities. Numerical modeling based on FEM is conducted. These numerical models are based on the experimental tests described by Villard and Briançon (2008). The numerical results are validated against the measured data of Villard and Briançon (2008) in terms of the load transfer, the surface settlement, the geosynthetic stress distribution, and the geosynthetic deflection. In addition, the effects of embankment height and cyclic loading are anticipated to enhance the understanding of load transfer mechanisms.

2 Description of Reference Case

The numerical analyses have been performed to model the full-scale experimental work on geosynthetic reinforced embankments over localized cavities by Villard and Briançon (2008), referred to as the reference case (see Fig. 1). The experiment was conducted on a rectangular trench measuring 30 m × 2.5 m. A rectangular cavity, 2 m long and 1 m wide, was arranged below the trench, filled with two balloons to simulate the cavity opening process by deflating the balloons. A geosynthetic reinforcement with a stiffness of 1100 kN/m was spread evenly along the trench, extending 30 m longitudinally.

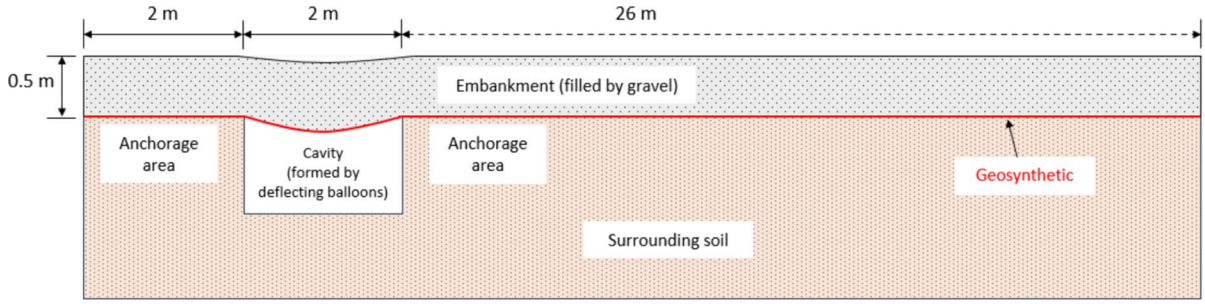

Fig. 1 Schema of cavity experiment in the study of Villard and Briançon (2008)

Compacted gravel, 0.5 m thick, was then placed over the geosynthetic. The cavity simulation was positioned on the left side of the experimental area. A limited-length cable-measuring device was used on the left side to measure the horizontal displacement of the geosynthetic. A detailed description of the site conditions, instrumentation, and monitoring devices was clearly presented in Villard and Briançon (2008). The testing procedure was carried out in three steps: (1) deflating the balloons to gradually create the cavity; (2) removing the deflated balloons to ensure that the geosynthetic was correctly positioned over the void; and (3) applying surcharge loads to the soil surface. During the tests, the horizontal displacement and strain of the geosynthetic were monitored.

3 Numerical Modeling

3.1 Description of Control Case

A 2D FEM model is developed to simulate the experimental work conducted by Villard and Briançon (2008), known as the control case. Due to the fact that the rectangular cavity was considered in the experiment, a plane strain model was employed in the numerical calculation. The study was conducted under drained conditions. Figure 2 shows the geometrical configuration of the model, where the overlying soil is modeled as a gravel layer and the surrounding soil has a length of 30 m, including 2.0 m in width of the cavity, 2.0-m length of the platform on the left side, and 26.0-m length on the right side. In the control case, the thickness of the gravel layer is 0.5 m, corresponding to an H/B ratio of 0.25. To investigate the influence of embankment height on the performance, the thickness of the gravel layer was increased to 6.0 m in this study. The geosynthetic material is placed between the overlying and surrounding soil, spanning a length of 30.0 m. The geosynthetic (GSY) is modeled by the linear elastic model, with a stiffness (J) of 1100 kN/m. As the load on the geosynthetic increases, the strain in the geosynthetic (ε) increases, and the tensile force (T) is generated according to the equation $T = J \times \varepsilon$. In the control case, the sudden opening process of the cavity is considered to simulate the process of sinkhole formation when inflating balloons. Other types of cavity openings are addressed in this study, which is presented in the testing program. The mesh was structured using 15-node triangular elements. When the soil or geosynthetics in the model are modeled under large deformations, the shape and location of elements in the computational grid may change. The mesh was updated from phase 1 to phase 4 to ensure continuous adjustment during large deformation analysis. The relative element size factor is used as 1.0 as the element distribution is set at the medium level and its dimension is 1.802. Regarding boundary conditions, the vertical boundaries were fixed in their normal directions. Meanwhile, the model bottom is fixed in both x and y directions, which means that no deformation is assumed below the surrounding soil. The coefficient of lateral earth pressure, K_0, was determined using the formula: $K_0 = 1 - sin(\varphi)$ (Jaky 1944). Following the experimental setup by Villard and Briançon (2008), a surcharge of 5.3 kPa is applied on the embankment top.

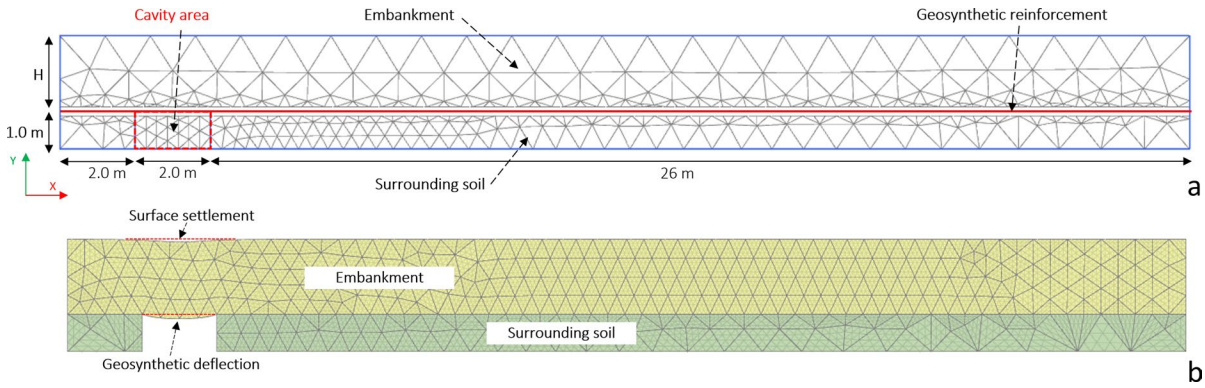

Fig. 2 Finite element mesh: Geometrical configuration (**a**); Numerical calculation (**b**)

3.1.1 Constitutive Models and Parameters

The complex system involves three different materials: surrounding soil, embankment (gravel fill), and geosynthetic. The soil materials were modeled as linear elastic-perfectly plastic materials, utilizing the Mohr–Coulomb failure criterion (MC model). The MC model was chosen due to its numerous advantages in achieving the research objectives (Pham and Dias 2021a; Pham et al. 2022; Vo et al. 2022). A notable advantage of the elastic-perfect plastic model is its ability to represent soils using well-established parameters, as presented in the referenced study (Villard and Briançon 2008). Due to its simplicity and effectiveness in representing the plasticity law and failure criterion of soil, the MC model has been used to simulate soil behavior under cyclic loading in some scenarios.

For instance, Wang and Ma (2007) used the MC model to develop and validate a simple soil model capable of handling complex loadings, including cyclic loading conditions. Achmus et al. (2009) and Kou et al. (2012) used the MC model to simulate the behavior of dense sand around monopile foundations of offshore wind turbines under cyclic loading. Kwon and Yoo (2020) also used the MC model to simulate the dynamic behavior of structures in liquefiable sand under cyclic loading conditions.

The geosynthetic material was modeled as a geogrid element, with isotropic linear elastic behavior. The interfaces were also defined using the Mohr–Coulomb failure criterion. The material models and parameters are summarized in Table 1.

3.1.2 Modeling Procedure

Cavities can form in several ways: (1) suddenly, when an underground cavity collapses; (2) gradually, through downward movement, subsidence, or sinking; and (3) progressively, over time, due to the erosion of soil or rock. To evaluate the effects of opening processes, both downward movement (Process D) and progressive opening (Process P) are simulated in addition to the sudden opening process (Process S) described in the control case. These simulations aim to investigate the influence of the cavity opening process on the reinforcement mechanism.

Concerning Process S (see Fig. 3a), the cavity is characterized by the sudden disappearance of the subsoil, which can occur in incidents involving underground structures. In Process D (Fig. 3b), the entire subsoil mass collapses vertically, representing a fixed opening diameter or width as the sinkhole develops. Process P (Fig. 3c) involves progressive subsidence, with the width or diameter of the cavity gradually increasing from the center.

The FEM simulation is conducted in five calculation steps. First, the surrounding soil, including the yielding mass of the cavity, is activated. Then, the geosynthetic is placed above the surrounding soil. Next, the gravel layer is placed to set up the embankment. The interfaces corresponding to the relevant materials are activated upon the appearance of these materials. With all components in place, the cavity is then induced to open using one of three processes. In Process S, the immediate disappearance of soil is modeled (see Fig. 3a). For Process D, the prescribed movement is applied for the opening process (see Fig. 3b). The movement continues until the deflected

Table 1 Input parameters for FEM models

Parameters	Symbol (unit)	Embankment (gravel material)	Surrounding soil	Interface gravel/ GSY	Interface GSY/ surrounding soil	Interface surrounding soil/surrounding soil
Material model		Mohr–Coulomb	Mohr–Coulomb	Mohr–Coulomb	Mohr–Coulomb	Mohr–Coulomb
Unit weight	γ (kN/m^3)	17	17	17	17	1
Young modulus	E' (kN/m^2)	20×10^3	22×10^3	20×10^3	22×10^3	1×10^3
Poisson's ratio	ν	0.2	0.3	0.2	0.3	0.3
Cohesion	c (kN/m^2)	1×10^{-3}	10	1×10^{-3}	10	1×10^{-1}
Friction angle	φ (°)	36	50	29	40	29
Dilatancy angle	ψ (°)	6	20	0	10	0

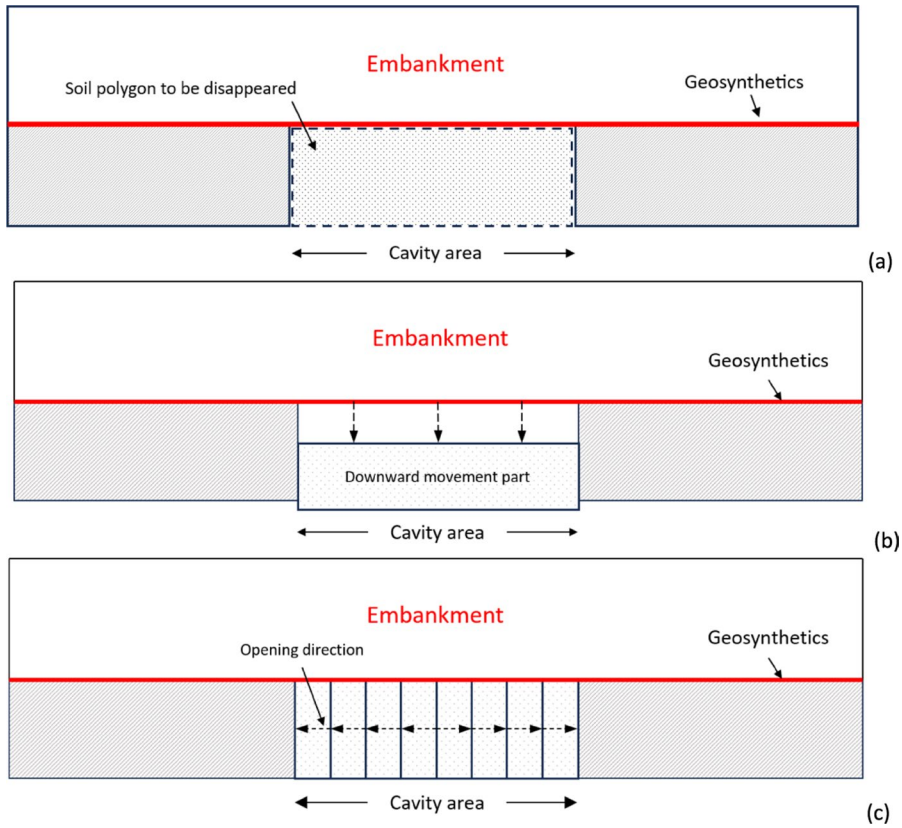

Fig. 3 Cavities open in different methods: **a** Process S–Sudden opening, **b** Process D–Downward opening, **c** Process P–Progressive opening

geosynthetic loses contact with the downward-moving part. In Process P, the opening method is simulated by deactivating several soil polygons, with progressively increasing the cavity width (see Fig. 3c). For all three processes, the cavity dimensions remain consistent.

After the cavity opens, a load is applied above the embankment. A key goal of this study is to determine how different loading conditions affect the system's behavior. The research involves applying a static load of 5.3 kPa on the embankment top, regarding the experimental conditions of the selected reference case. In the FEM simulation program (PLAXIS 2020), a harmonic signal is used to define the cyclic load, as presented in Eq. (2).

$$F = \hat{M}\hat{F}sin\left(\omega t + \varphi_0\right) \tag{2}$$

where $\hat{M}\hat{F}$ is the amplitude of cyclic load, $\omega = 2\pi f$, with f is the frequency (Hz), φ_0 is the initial phase angle (degrees). The effect of cyclic loading is studied at varying frequencies corresponding to N cycles (1, 5, 10, 50, and 100). Similar cyclic loading configurations have been employed in studies conducted by Pham et al. (2018b), Pham and Dias (2021b), Houda et al. (2016), and Houda et al. (2019). Throughout the phase of cyclic loading, the amplitude value for the cyclic load remains constant at 5.3 kPa.

To simulate sinkhole occurrence, several interfaces are defined for interactions between different materials. The primary interfaces are Gravel/GSY, Surrounding soil/GSY, and Surrounding soil/Surrounding soil. The interface characteristics are based on the fill material, using a shear strength reduction ratio of 0.8 ($\varphi_{interface} = 0.8 \times \varphi_{soil}$) as suggested by previous studies (Villard et al. 2016; Pham 2019; Pham and Dias 2021a). Concerning Process D, the "Surrounding soil/Surrounding soil" interface is assigned very low stiffness to allow movement between the yielding mass and adjoining mass of the surrounding soil. Different interfaces are used for the various cavity opening methods, as shown in Fig. 4a for Process S and P, and Fig. 4b for Process D.

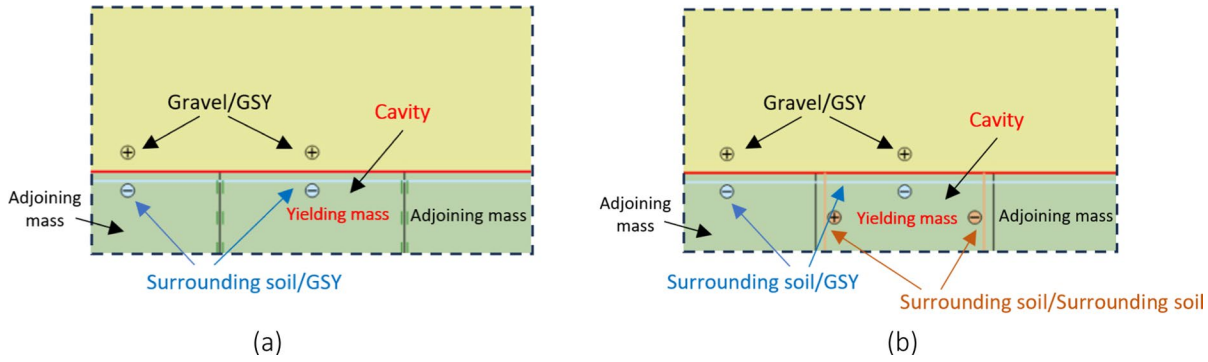

Fig. 4 Interfaces used in the numerical models: **a** Processes S and P, **b** Process D

3.2 Validation of FEM Simulation

The full-scale experiment conducted by Villard and Briançon (2008) served as the basis for validating the FEM model developed to analyze geosynthetic-reinforced embankments subjected to localized cavities. In addition to their experimental work, Villard and Briançon (2008) performed numerical simulations to replicate the experimental findings. To validate the current model, the geosynthetic deflection calculated by FEM analysis was compared with both field measurements and the numerical results reported by Villard and Briançon (2008).

Figure 5 illustrates the comparison between geosynthetic deflection obtained from current FEM analysis, referenced numerical results, and field measurements. The FEM results show geosynthetic deflection consistent with the field-measured data. The observed geosynthetic deflection was approximately 0.23 m, compared to 0.24 m obtained from the simulation. Furthermore, as shown in Fig. 5, the FEM results closely align with the numerical results presented by Villard and Briançon (2008). A third-order polynomial function was used to fit the geosynthetic deflection, with coefficients of determination (R^2) of 0.999, 1, and 0.997 for FEM, referenced numerical, and experimental methods,

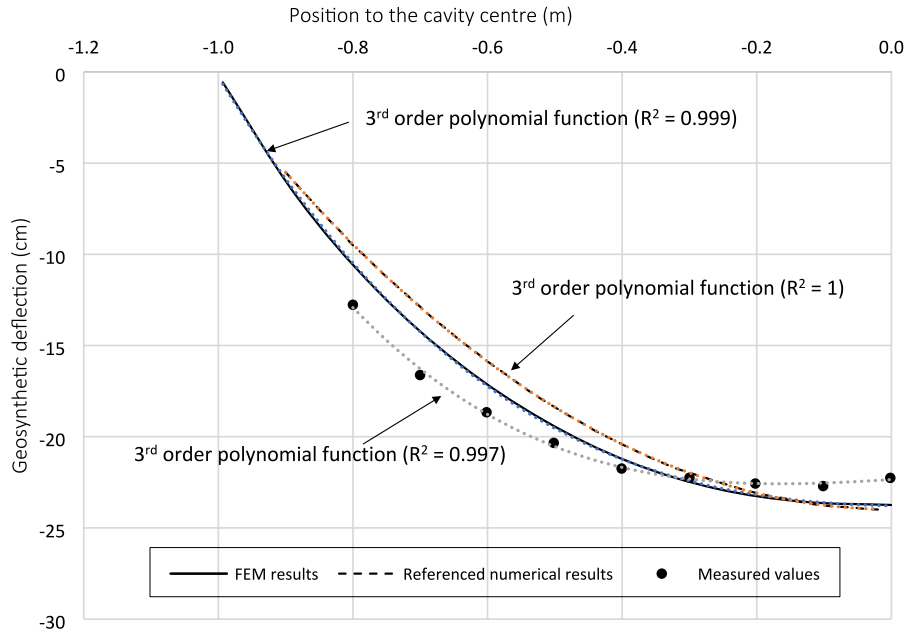

Fig. 5 Geosynthetic deflection obtained by experiment and numerical modeling

respectively. The nearly perfect R^2 values indicate a very high degree of fit between the numerical models and the experimental data. This demonstrates that a third-order polynomial function can accurately capture the complex deflection patterns of geosynthetics, offering significant benefits for both numerical modeling and the optimization of current design methods. These findings are in good agreement with the conclusion from Pham et al. (2018a), where the polynomial curve was confirmed to fit well the geosynthetic deflection shape in a physical experiment.

Moreover, the similarity between the numerical and experimental results highlights the reliability of FEM models in analyzing and designing geosynthetic reinforcement systems. This is particularly important in practical applications where the accurate prediction of material behavior is essential to ensure safety and economic efficiency. Overall, these findings validate the accuracy of the current FEM model and suggest that numerical methods can be widely and effectively applied in geosynthetic-related research and applications.

4 Results and Discussion

4.1 Deformation Analyses Under Different Cavity Opening Processes

In the field study conducted by Villard and Briançon (2008), the cavity opening process was simulated by inflating balloons, though the exact speed of this process was not specified. As a result, the simulated cavity opening process differed from natural cavity formation, introducing certain limitations. The deformation mechanism within the reinforced system is significantly influenced by the nature of the cavity-opening process. To better understand the deformation within the geosynthetic-reinforced embankment under different opening procedures, three types of process (Process D, Process P, and Process S) are studied.

Figure 6 presents the numerical results of vertical deformation including surface settlement and geosynthetic deflection, in geosynthetic reinforced embankment over a cavity. The surface settlement and geosynthetic deflection exhibit a parabolic shape, with the maximum values occurring along the centerline. As previously discussed, the geosynthetic deflection in Process S closely matches the measured data

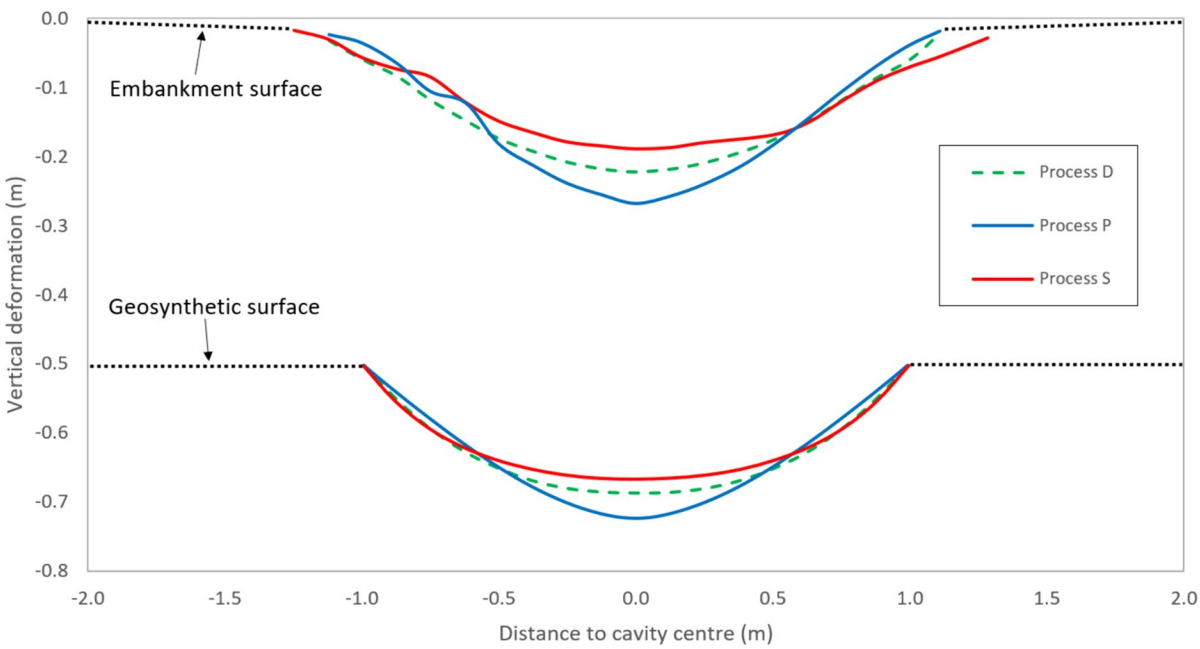

Fig. 6 Vertical deformation within embankment under different cavity opening

from the full-scale experiment in the control case. In addition, the vertical deformation is different with the different opening methods. In Process P, both the surface settlement and the geosynthetic deflection reach critical values due to the cavity opening. Specifically, settlement in Process P is 19% greater than in Process D and 27% greater than in Process S. Concerning the geosynthetic deflection, Process P shows a 13% increase compared to Process D and a 23% increase compared to Process S. The key difference between the three opening procedures, as revealed by the numerical analyses, lies in the rate of cavity formation. The results clearly indicate that the opening process is crucial for accurately defining both surface settlement and geosynthetic deflection.

The dependence of the deformation mechanism on the cavity opening process has been realized by Villard et al. (2016) and Pham et al. (2018a). To focus on the most critical scenarios in the reinforcement system while optimizing calculation time, the numerical analyses focus on the two primary cavity opening processes: Process P and Process D.

4.2 Geosynthetic Deflection

While geosynthetic tensile stiffness is a critical property, its value in the control case is already sufficiently high, meaning that further increases have a minimal impact on reducing settlement (Benmebarek et al. 2015). Therefore, in the results presented below, the geosynthetic strength value is maintained as set in the control case.

Figure 7 illustrates the maximum geosynthetic deflection under two different cavity opening processes, considering both static and cyclic loading effects. The results clearly indicate that cyclic loading leads to geosynthetic deflection compared to static loading. Notably, while both Process P and Process D result in increased deflection under cyclic loads, Process P consistently leads to greater deformation. The difference in geosynthetic deflection between static and cyclic loads is more pronounced in Process P, with a maximum difference of 7%, compared to 4% in Process D. Additionally, in Process P, a threshold is observed at 10 cycles, beyond which the increase in geosynthetic deflection becomes more gradual. As the cycle number reaches 200, the changes in deflection become negligible, indicating a stabilization in geosynthetic deformation.

As shown in Fig. 7, for a single load cycle (N = 1), the difference between responses to static and cyclic loads is minimal. This difference can be attributed to numerical effects and the inherent differences in how static and cyclic loads apply stress to the system. Even during the first load cycle, the nature of the load application can induce different initial responses in the material or structure being analyzed. A similar finding was also observed in the study by Houda et al. (2016).

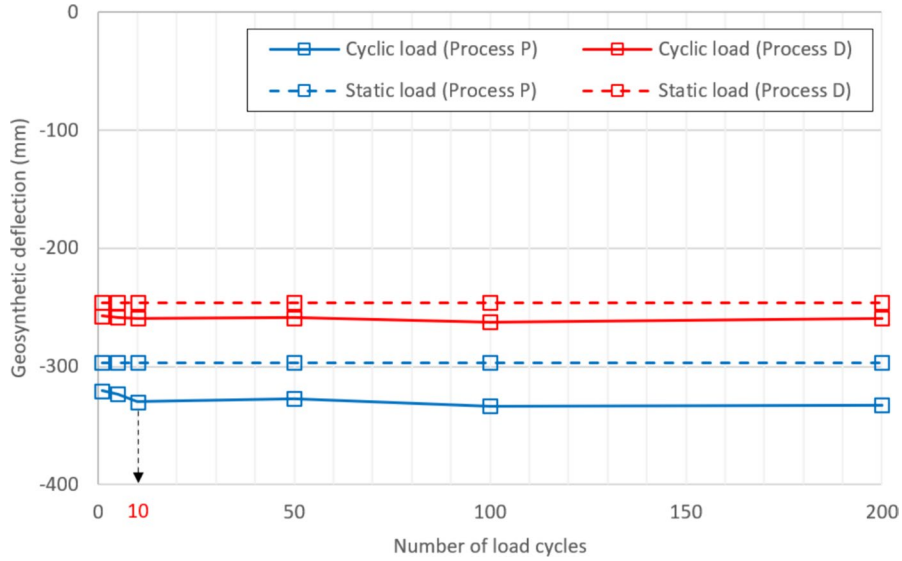

Fig. 7 Maximum geosynthetic deflection under different load types

The obtained shapes of geosynthetic deflection under static and cyclic loads (with N = 50) using the two numerical opening processes are presented in Fig. 8. As can be seen in the figure, the black dotted curves represent third-order polynomial functions that fit the numerical results for the geosynthetic deflection under different loading conditions. These curves provide a mathematical representation of the relationship between the distance to the cavity center and the geosynthetic deflection for both cyclic and static loads under processes P and D. The high R^2 values (0.98 and 0.99) confirm the strong fit of the polynomial functions. It is interesting to note that the loading condition has no effect on the shape of the geosynthetic deflection. The difference between the shapes of geosynthetic deflection under the two opening processes is relevant to the distributed load on the geosynthetic over cavity, which is analyzed in the following sections.

Considering a given cavity width, the influence of embankment height is also considered to affect the behavior of geosynthetics, as indicated in Fig. 9. Numerical results show that the effect of embankment height on settlement is different with the cavity opening process and the loading condition. In fact, for each ratio of H/B, the geosynthetic deforms more in the case of Process P with both loading conditions. The effect of cyclic loading causes more deflection in geosynthetics with all the embankment heights. However, the difference in deformation between cyclic and static loads is clearly noted in the case of cavity opening in Process P. Especially, in the case of H/B of 0.5, the vertical deformation of geosynthetic reaches the maximum value in the case of Process P, and the cyclic loading causes deformation 16% larger than static loading. The differential influence on geosynthetic deformation between cyclic and static loading seems to remain in the case of Process D, meanwhile, it has a slight fluctuation with embankment height in the case of Process P.

A consistent trend across H/B ratios can be seen in Fig. 9. For both processes, the geosynthetic

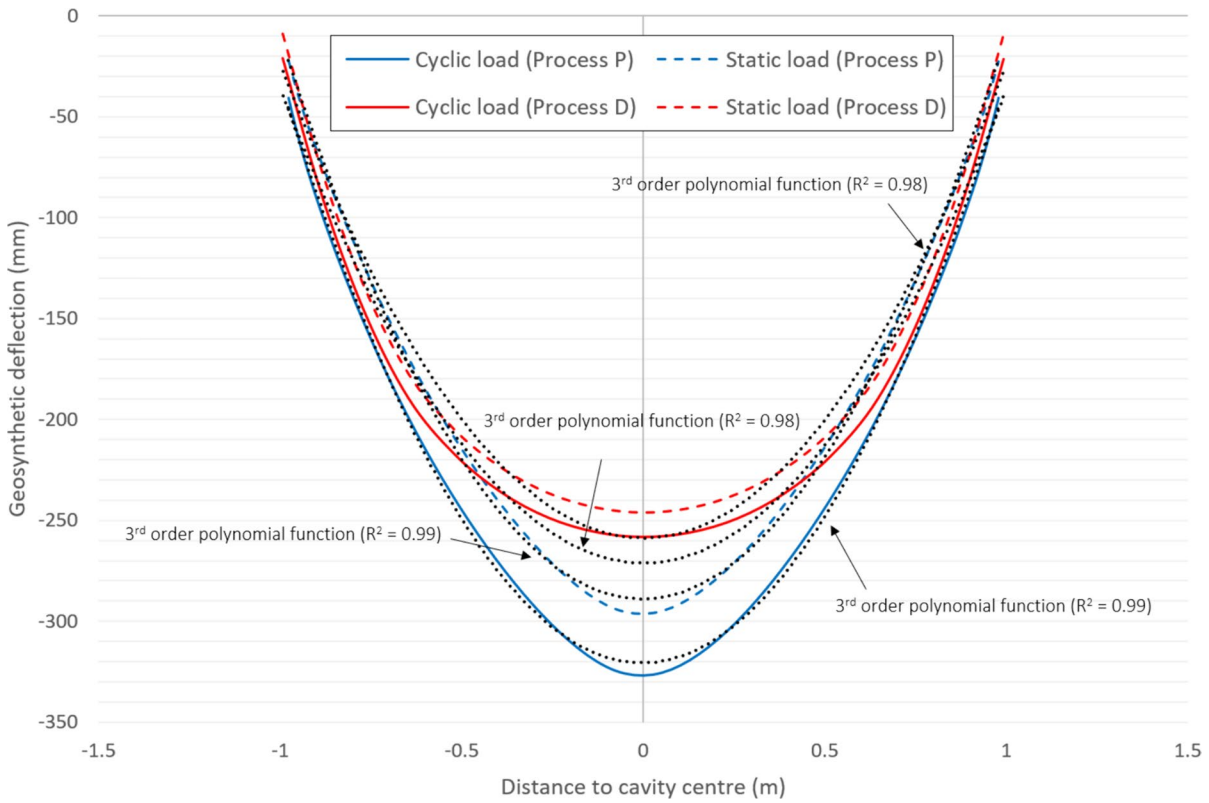

Fig. 8 Shape of geosynthetic deflection under static and cyclic loads (N = 50)

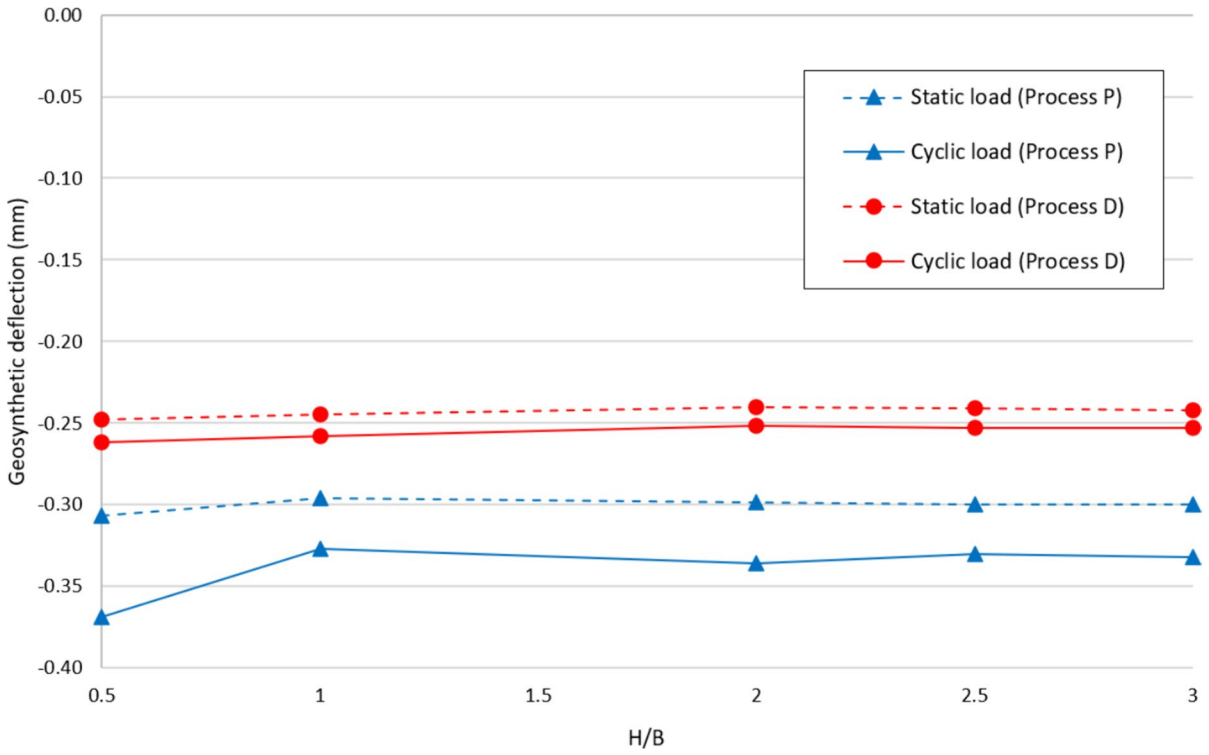

Fig. 9 Influences of embankment height on geosynthetics deflection under static and cyclic loads (N = 50)

deflections remain relatively stable under static and cyclic loads, suggesting that embankment height does not significantly influence deformation in these scenarios. Similar results were observed in the experimental study by Pham et al. (2018a) and the numerical study by Pham et al. (2022). This stability can be attributed to the variation in load distribution on the geosynthetic surface with different embankment heights, which is discussed in the following section.

4.3 Surface Settlement

The surface soil settlement obtained from numerical results is shown in Fig. 10 under two types of loading conditions. Cyclic loading results in larger settlements compared to static loading across the cavity opening processes. However, the difference between loading conditions can be noticed in the cases of Process P and Process D. In fact, cyclic loading increases the surface settlement by a maximum of 9% compared to static loading in the case of Process P, which is only 3% in the case of Process D. Furthermore, under cyclic loading, the number of load cycles appears to have minimal impact on the overall settlement of the embankment.

The shapes of the surface settlement in the cavity range obtained from numerical simulation are presented in Fig. 11. The numerical results indicate that similar settlement profiles are observed across the two loading types and cavity opening processes. A 4th-order polynomial function is fitted to the obtained shapes with the determination coefficient of 1.0. It should be noted that cyclic loading (with a considered N of 50) has no effect on the deformation shape of the embankment surface compared to static loading.

Figure 12 presents the influence of embankment height on the surface settlement under different loading types. The influence of cyclic loading compared to static loading is more significant in Process P than in Process D. Significant settlements are obtained when the embankment height (H/B ratio) increases. It is interesting to note that, under the two types of opening processes and the two loading conditions, the threshold height of the embankment, as indicated by the relevant H/B ratio of 2.0, is reached. The variations of settlement are present in Table 2. As the H/B

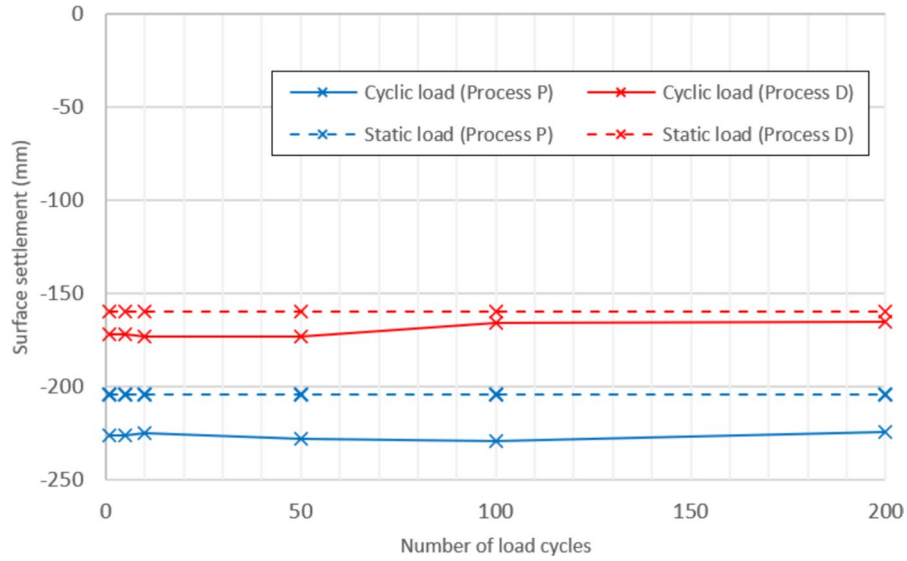

Fig. 10 Maximum surface settlement under different load types

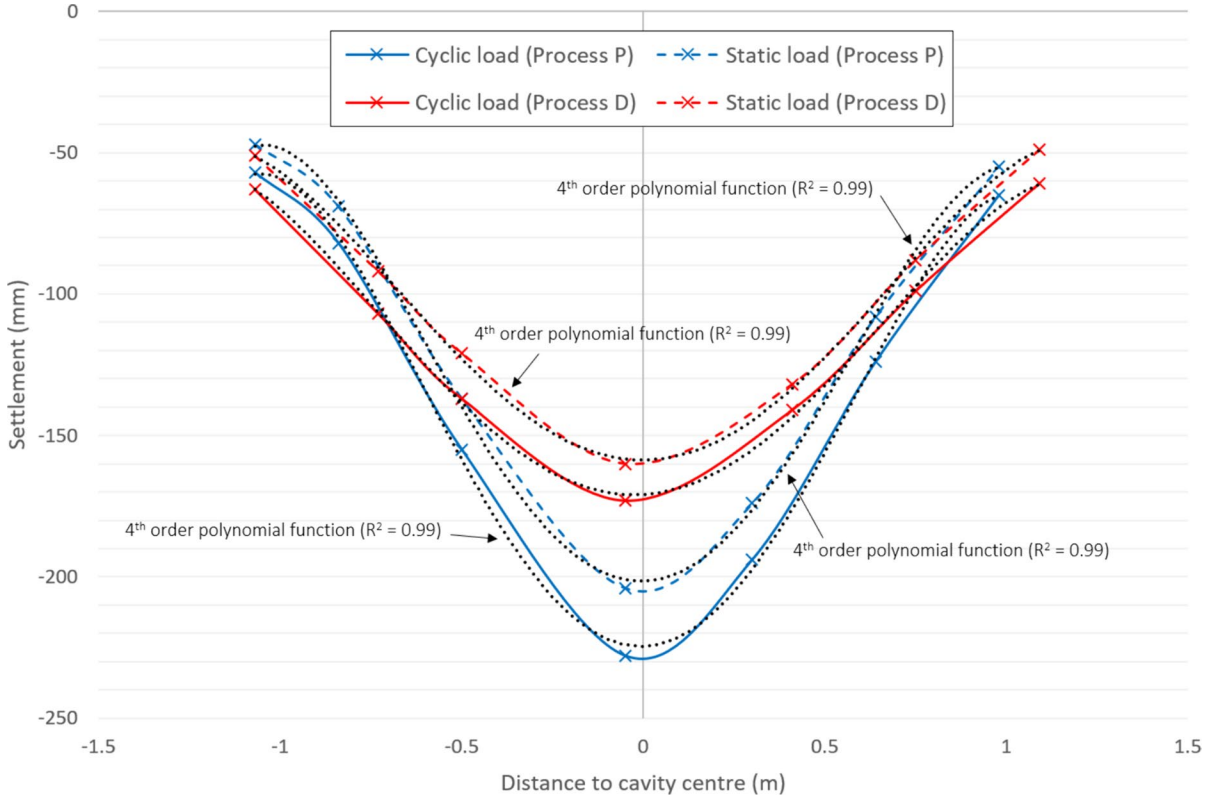

Fig. 11 Shape of surface settlement under under static and cyclic loads (N = 50)

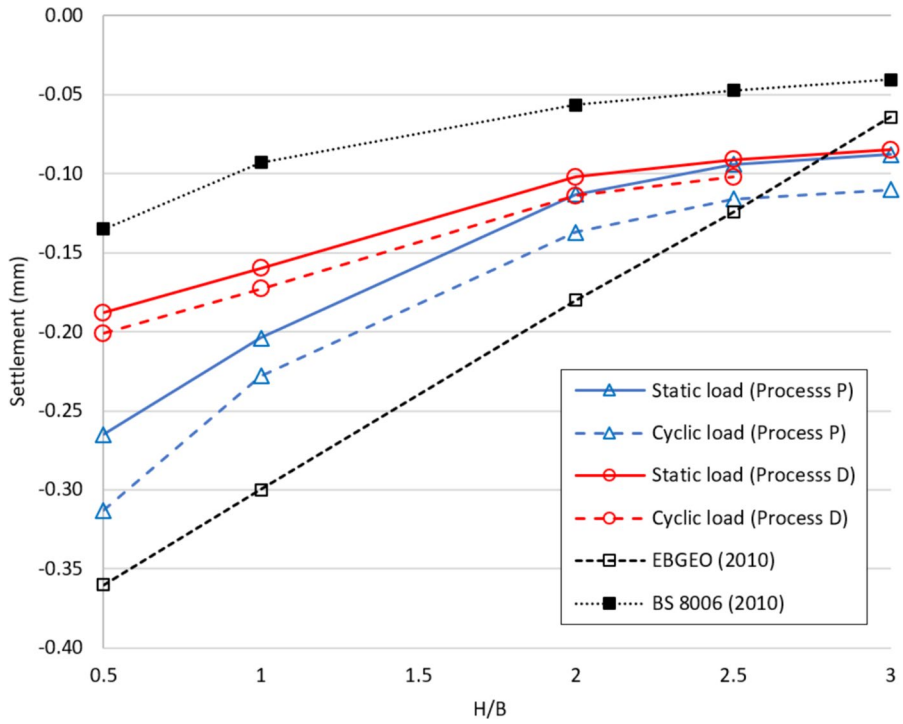

Fig. 12 Influences of embankment height on surface settlement under static and cyclic loads (N = 50)

Table 2 Settlement variation under different testing conditions

Testing conditions	Low embankments	Heigh embankments
Process P + Static loading	57%	22%
Process P + Cyclic loading	56%	20%
Process D + Static loading	46%	17%
Process D + Cyclic loading	43%	14%

ratios are less than 2.0, the maximum decrease in settlement is very large, with an increase of 57%. On the contrary, as the H/B ratio is larger than 2.0, the maximum change in settlements is rather small, with an increase of 22%. This confirms the critical embankment height, which is related to the load transfer efficacy.

Figure 12 also compares the numerical results with analytical predictions from BS 8006 (2010) and EBGEO (2010). BS 8006 demonstrated a significant underestimation of surface settlement, due to the fact that the method was proposed from simplified assumptions including no soil arching and a constant volume of depression soil within the embankment. Meanwhile, EBGEO (2010) showed a linear correlation between the calculated settlement and the embankment height. As the H/B ratio is less than 2.5, EBGEO (2010) predicts a larger settlement than the numerical simulation. However, for the case of H/B of 3.0, the analytical results are lower than the numerical ones. It should be noted that these design methods suggest using constants in the design process and do not take into account the influence of loading conditions and the process of cavity opening.

4.4 Load Transfer Analysis

Regarding the effects of static loading and cyclic loading number, the numerical results of load transfer efficacies are computed following Eq. 1 for the different cavity opening processes. The load transfers more efficiently in the case of Process P than in Process D. This is observed for both cyclic and static loading cases. Comparing the two loading types, it can be concluded that the cyclic load causes less effective load transfer. However, this influence is minimal for load cycles of fewer than 10. This finding is consistent with the effect of a number of load cycles on geosynthetic deflection, as presented in Fig. 7. In fact, larger load cycles decrease the load transfer efficacies,

and this allows more load to exist on the cavity area and causes large geosynthetic deflection.

The distributed stress developed from the embankment fill applied along geosynthetic reinforcement under different loading conditions is computed in both opening processes. The applied stress above the geosynthetic is determined from the stress values along the upper interfaces of the geosynthetic on the cavity area. The numerical results are presented in Fig. 13a and b for cases of Process P and Process D, respectively. The stress applied to the anchorage areas is significantly larger than that applied to the cavity areas in both opening processes. This confirms that the load transfer phenomenon is reproduced well in the numerical models. In Process P, the stress distribution assumes a cone-like shape, with higher stress concentrated at the cavity center compared to the surrounding areas (Fig. 13a). On the other hand, the shape of stress distribution is like a parabola as the distributed stress at the cavity center reaches the lowest value in Process D (Fig. 13b). There is no difference in every loading condition, between the static load and the cyclic load including the difference in the number of cyclic loads affecting the shape of distributed stress. The difference in shape due to opening processes can be explained that during the cavity opening, the load transfer mechanism is changed followed by a continual increase of cavity width (Process P) and the downward movement of the opening process (Process D) seems not to affect the load distribution.

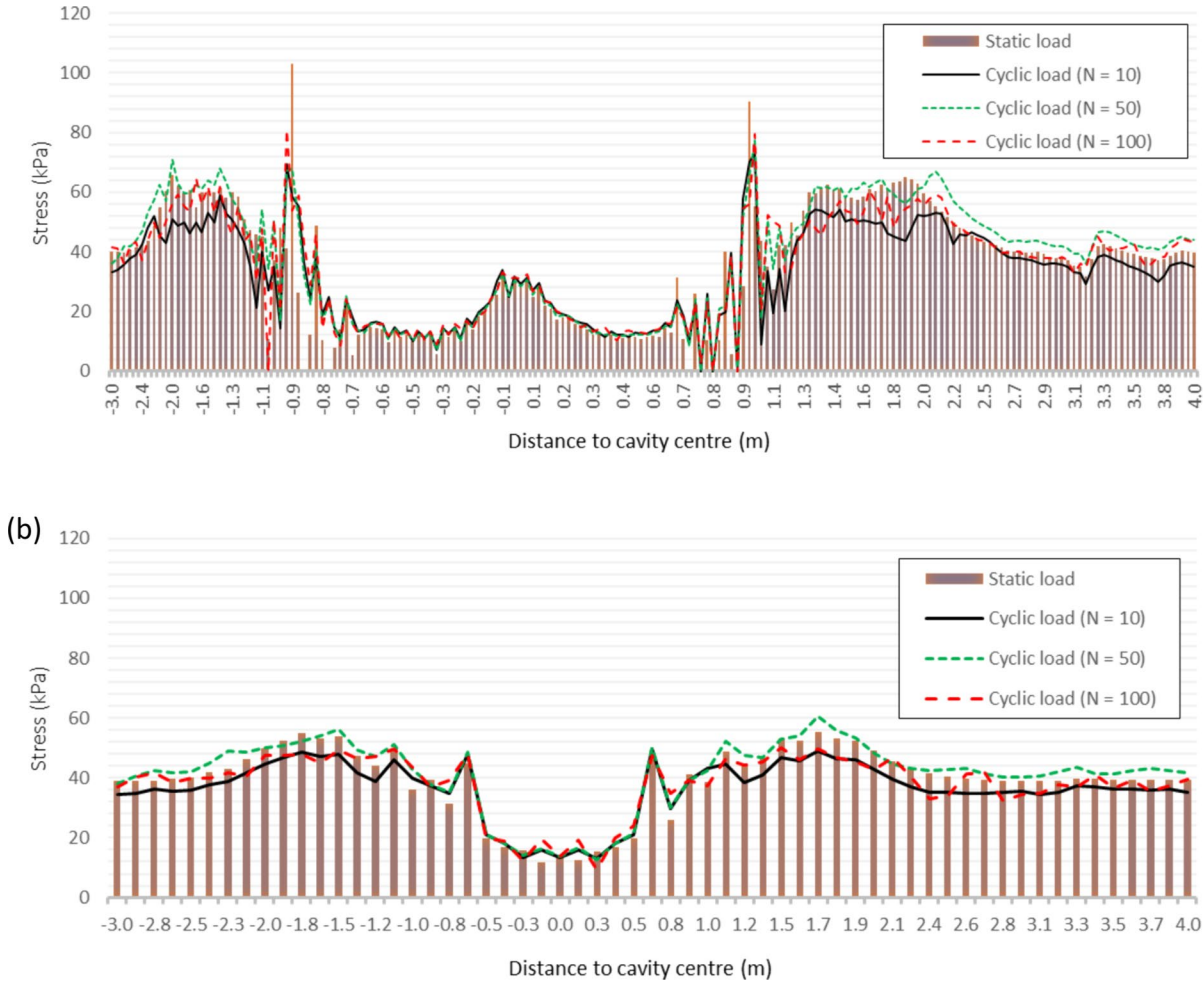

Fig. 13 Shape of distributed stress over cavity: **a** Process P, **b** Process D

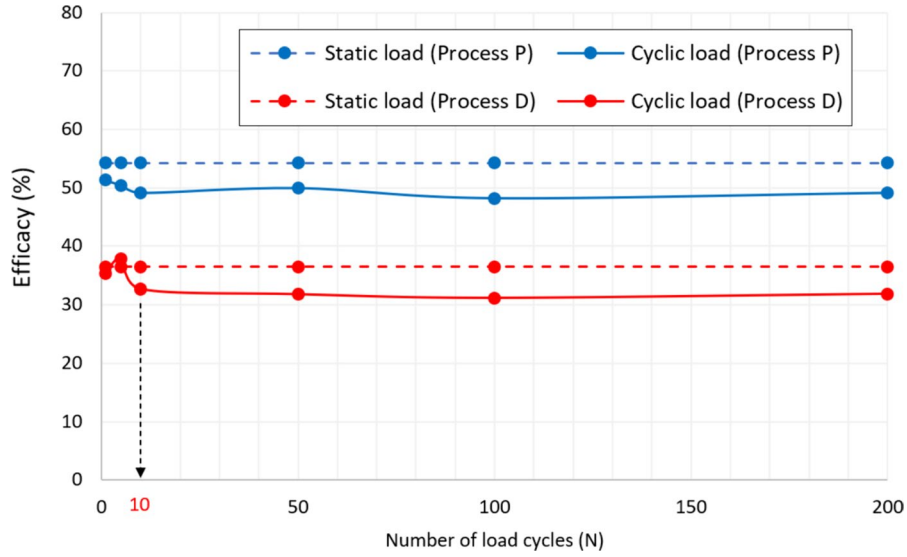

Fig. 14 Load transfer efficacies under different load types

This finding also explains the influence of cavity opening on the geosynthetic deflection, as presented in Fig. 8, whereas the load transfer efficacy in the case of Process P is greater than that of Process D (Fig. 14). In fact, the load at the cavity center in the case of Process P is greater than that of Process D, in which the load is transferred close to the cavity edge.

Regarding two loading conditions, Fig. 15 presents that load transfer efficacy increases with higher embankment under two different cavity opening processes. The shear resistance of filling soil in the high embankments is mobilized more than that in low embankments. This mobilization enhances soil arching within the embankment, leading to more efficient load transfer to the anchorage area as embankment

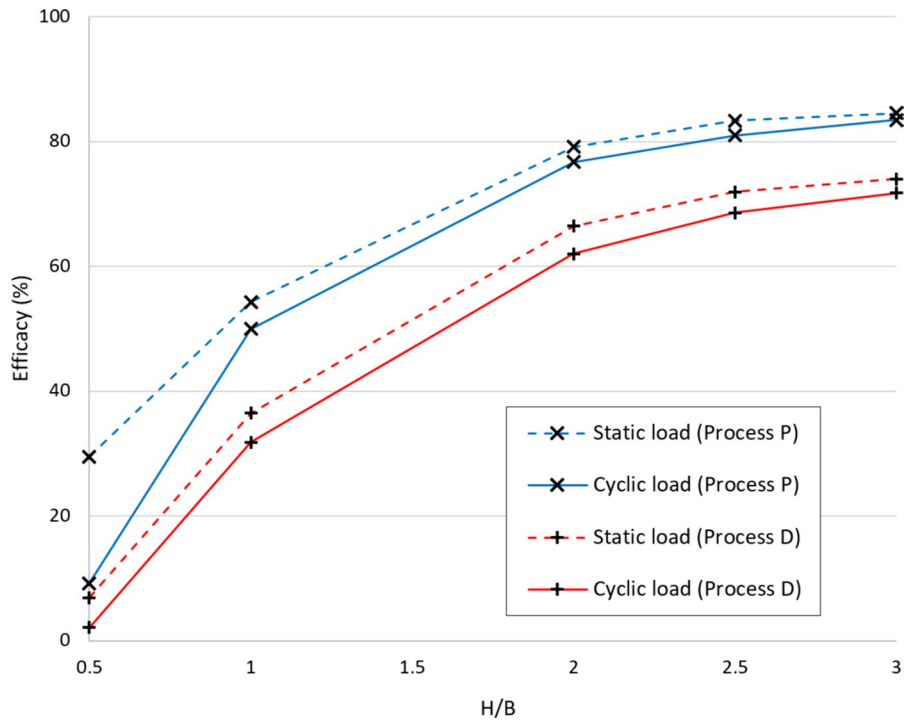

Fig. 15 Influences of embankment height on efficacy of load transfer under static and cyclic loads (N = 50)

height increases, rather than increasing stress on the geosynthetic material. This efficient load transfer mechanism explains why an increase in embankment height does not result in a corresponding increase in the deflection of the geosynthetic, as presented in Fig. 9. The critical height of the embankment is noticed corresponding to the value of H/B equal to 2.0. In fact, with a H/B ratio larger than 2, the efficacy variation is less than 13%, meanwhile, it is over 90% for low embankments. These results are compatible with the settlement analysis results under the influence of embankment height in Fig. 12. To conclude, the critical embankment height in numerical analyses is just greater than 2 times the cavity width. This finding is slightly smaller than the value of 2.5 found in the study conducted by Terzaghi (1943). Note that, the nonexistence of geosynthetic reinforcement in that study resulted in the high critical height.

4.5 Estimation of Load Transfer Efficacy Based on FEM Simulations

The current numerical investigation estimates load transfer efficacy by considering the impact of the H/B ratio. As illustrated in Fig. 16, the computed load transfer efficacies are shown for various load types and cavity opening methods, in which the variation of the H/B ratio is considered. The formula for calculating load transfer efficacy is expressed by the power function in Eq. 3. The determination coefficient for the proposed equation is 0.92. It should be noted that in the numerical analyses, a cavity width of 2 m was used.

$$E = 37.92\left(\frac{H}{B}\right)^{0.74} \tag{3}$$

In order to verify the proposed load transfer efficacy equation, the two previous experiments are selected. Based on the full-scale experiment, Villard et al. (2016) conducted a numerical study to consider a circular sinkhole with a diameter of 2.2 m. Pham et al. (2018a) conducted a small-scale experiment considering a circular cavity with a diameter of 0.5 m. Both studies were focused on the load transfer mechanism within the reinforced fill material over the cavity area considering influences of the cavity opening process. Typical cases are selected for the validation, including one test with a H/B ratio of 2.5 used by Villard et al., (2016) and a H/B ratio of 0.5 chosen by Pham et al. (2018a), and the corresponding load transfer efficacy values are 87% and 23%, respectively. Figure 16 shows that the load transfer efficacy calculated by the proposed equation differs by 14% from the value reported by Villard et al. (2016). Meanwhile, the experiment results conducted by Pham et al. (2018a) are in close agreement with those predicted by the proposed equation, with a difference of 1%. It is evident that the predicted results by the

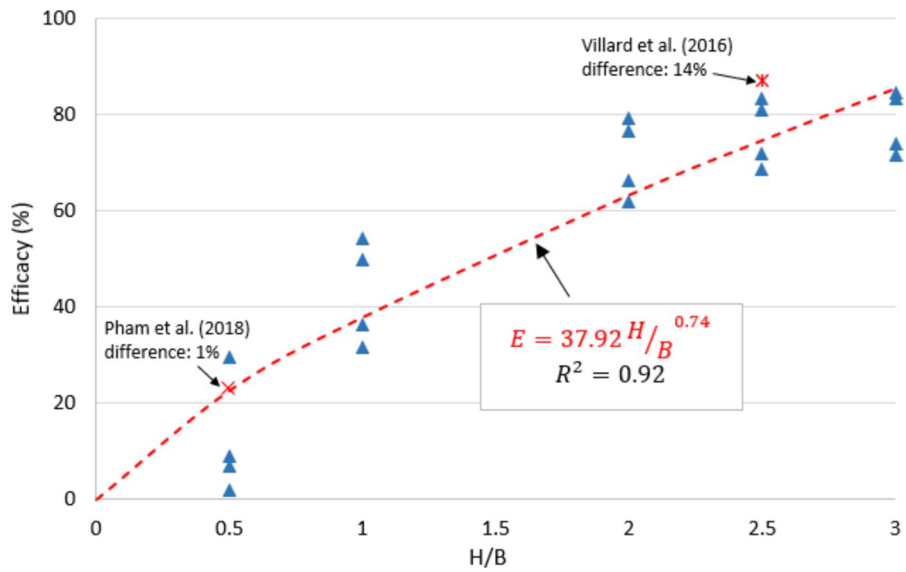

Fig. 16 Modification of efficacy of load transfer based on the numerical results

proposed equation fit well with the referenced efficacy values. Hence, the proposed equation provides a dependable means of assessing load transfer efficacy within the reinforced embankment over the cavity. This finding suggests that the proposed equation can accurately estimate vertical stress on geosynthetics in the cavity area.

5 Conclusions

In this study, a series of finite element models were developed to investigate the load transfer mechanisms in granular embankments reinforced by geosynthetics over cavities, considering the influences of different cavity opening methods and cyclic loadings. The numerical results led to the following conclusions:

- The numerical results for geosynthetic deflection were well-validated against experimental data and referenced numerical results from Villard and Briançon (2008).
- The cavity opening process had a significant impact on the surface settlement, the geosynthetic deflection, and the stress distribution. Progressive opening caused the highest deformations and the most effective load transfer, while increasing-width cavity formation led to substantial surface deformation and geosynthetic deflection, producing a cone-shaped stress distribution. In contrast, downward movement resulted in a parabolic stress distribution.
- Cyclic loading increased both surface settlement and geosynthetic deflection while reducing the overall load transfer efficacy.
- The critical embankment height corresponds to an H/B ratio of 2.0, it is not unaffected by loading conditions.
- The load transfer efficacy for geosynthetic-reinforced embankments over cavities is described using a power function. To validate the proposed function, efficacy shows a difference in the range of 1.0%–14.0% in relevant studies.

Future research should focus on developing three-dimensional numerical models for circular cavities, exploring various constitutive models for fill materials, and examining the effects of higher surcharges and cyclic load amplitudes. Practical experiments are recommended to further validate the proposed function for estimating load transfer efficacy.

Acknowledgements We would like to thank Ho Chi Minh City University of Technology (HCMUT), VNU-HCM for the support of time and facilities for this study.

Author Contribution MTP: Conceptualization, Investigation, Methodology, Validation, Writing—original draft. DDN: Conceptualization, Investigation. TDN: Investigation, Editing. VHP: Methodology, Writing—review & editing, Conceptualization and General Supervision All authors have read and agreed to the published version of the manuscript.

Funding The authors have not disclosed any funding.

Data Availability Some or all data, models, or code that support the findings of this study are available from the corresponding author upon reasonable request.

Declarations

Conflict of interest The authors state that there are no conflicting interests that could inappropriately bias this work, and the authors still declare their interest in the development of this research.

References

Achmus M, Kuo YS, Abdel-Rahman K (2009) Behavior of monopile foundations under cyclic lateral load. Comput Geotech 36:725–735. https://doi.org/10.1016/j.compgeo.2008.12.003

Agaiby S, Jones C (1996) Design of reinforced fill systems to support footings overlying cavities. Geotext Geomembr 14:57–72. https://doi.org/10.1016/0266-1144(96)00005-2

Benmebarek S, Berrabah F, Benmebarek N (2015) Effect of geosynthetic reinforced embankment on locally weak zones by numerical approach. Comput Geotech 65:126–135. https://doi.org/10.1016/j.compgeo.2014.12.004

Blivet J, Gourc J, Villard P, Giraud H, Khay M, Morbois A (2002) Design method for geosynthetic as reinforcement for embankment subjected to localized subsidence. In: proceedings of the seventh international conference on geosynthetics, Nice, France, September 2002, pp 163–171

Bonaparte R, Berg RR (1987) The use of geosynthetics to support roadways over sinkhole prone areas. In: proceedings of the second multidisciplinary conference on sinkholes and the environmental impacts of karst, Orlando, FL, February 1987, pp 437–445

Brahmi S, Fehdi C, Hadji R, Brahmi S, Amor H, Hamed Y (2023) Karst-induced sinkhole detection using a tomography imaging survey, case of Setifian high plain, NE Algeria. Geotech Geol Eng 41:1234–1246. https://doi.org/10.1007/s10706-023-02384-x

Briançon L, Villard P (2008) Design of geosynthetic-reinforced platforms spanning localized sinkholes. Geotext

Geomembr 26:416–428. https://doi.org/10.1016/j.geotexmem.2007.12.005
British Standards Institution (2010) Code of practice for strengthened/reinforced soils and other fills. BS 8006:2010. British Standards Institution, London. ISBN 978-0-580-53842-1
Chalak C, Briançon L, Villard P (2019) Coupled numerical and experimental analyses of load transfer mechanisms in granular-reinforced platform overlying cavities. Geotext Geomembr 47:413–428. https://doi.org/10.1016/j.geotexmem.2019.04.003
da Silva B, Elshafie MZEB (2021a) Geosynthetic-reinforced soils above voids: observation of soil and geosynthetic deformation mechanisms. Geotext Geomembr 49:1–18. https://doi.org/10.1016/j.geotexmem.2020.02.013
da Silva B, Elshafie MZEB (2021b) Geosynthetic-reinforced soils above voids: observation and prediction of soil arching. Geotext Geomembr 49:579–592. https://doi.org/10.1016/j.geotexmem.2020.11.005
El Ganainy H, Demirkan M, Gutierrez J, Ramanathan R, Hatipoglu B, Adib M, Barton D (2016) Stability of solution cavities in urban developments: a case study towards enhancing geohazard risk assessment. Geotech Geol Eng 34:85–97. https://doi.org/10.1007/s10706-015-9933-1
Gabr MA, Hunter TJ (1994) Stress-strain analysis of geogrid-supported liners over subsurface cavities. Geotech Geol Eng 12:65–86. https://doi.org/10.1007/BF00429767
German Geotechnical Society (2010) Recommendations for design and analysis of earth structures using geosynthetic reinforcements (EBGEO). 2nd edn. Ernst & Sohn, Berlin. ISBN 978-3-433-02950-3
Giroud JP (1981) Designing with geotextiles. Materiaux et Constructions 14:257–272
Giroud JP, Bonaparte R, Beech JF, Gross BA (1990) Design of soil layer-geosynthetic systems overlying voids. Geotext Geomembr 9:11–50. https://doi.org/10.1016/0266-1144(90)90004-V
Giroud JP, Bonaparte R, Beech JF, Gross BA (1988) Load carrying capacity of a soil layer supported by a geosynthetic overlying a void. In: proceedings of the international geotechnical symposium on theory and practice of earth reinforcement, Fukuoka/Kyushu, Japan, October 1988, pp 185–190
Girout R, Blanc M, Dias D, Thorel L (2014) Numerical analysis of a geosynthetic-reinforced piled load transfer platform-validation on centrifuge test. Geotext Geomembr 42:525–539. https://doi.org/10.1016/j.geotexmem.2014.07.012
Gutiérrez F, Johnson KS, Cooper AH (2008) Evaporite karst processes, landforms and environmental problems. Environ Geol 53:935–1105. https://doi.org/10.1007/s00254-007-0715-9
Han G, Gong Q, Zhou S (2015) Soil arching in a piled embankment under dynamic load. Int J Geomech 15:04014094. https://doi.org/10.1061/(ASCE)GM.1943-5622.0000443
Han G, Gong Q, Zhou S (2011) Mechanical analysis of soil arching under dynamic loads. In: proceedings of the 2011 Pan-Am CGS geotechnical conference, Toronto, ON, Canada, 2–6 October 2011
Hewlett WJ, Randolph MF (1988) Analysis of piled embankment. Ground Eng 21:12–18
Houda M, Jenck O, Emeriault F (2016) Physical evidence of the effect of vertical cyclic loading on soil improvement by rigid piles: a small-scale laboratory experiment using digital image correlation. Acta Geotech 11:325–346. https://doi.org/10.1007/s11440-014-0350-z
Houda M, Emeriault F, Jenck O (2019) Rigid pile improvement under vertical cyclic loading: 1 g laboratory small scale modelling. Int J Phys Model Geotech 19:89–103. https://doi.org/10.1680/jphmg.16.00040
Huckert A, Briançon L, Villard P, Garcin P (2016) Load transfer mechanisms in geotextile-reinforced embankments overlying voids: experimental and analytical approaches. Geotext Geomembr 44:442–456. https://doi.org/10.1016/j.geotexmem.2015.06.005
Jaky J (1944) The coefficient of earth pressure at rest. J Soc Hung Archit Eng 3:355–358
Kou YS, Achmus M, Abdel-Rahman K (2012) Minimum embedded length of cyclic horizontally loaded monopiles. J Geotech Geoenviron Eng 138:357–363. https://doi.org/10.1061/(ASCE)GT.1943-5606.0000602
Kwon S, Yoo M (2020) Study on the dynamic soil-pile-structure interactive behavior in liquefiable sand by 3D numerical simulation. Appl Sci 10:82723. https://doi.org/10.3390/app10082723
Pham AT, Dias D (2021a) 3D numerical study of the performance of geosynthetic-reinforced and pile-supported embankments. Soils Found 61:1319–1342. https://doi.org/10.1016/j.sandf.2021.07.002
Pham VH, Dias D (2021b) 3D Numerical modeling of rigid inclusion-improved soft soils under monotonic and cyclic loading case of a small-scale laboratory experiment. Appl Sci 11:1426. https://doi.org/10.3390/app11041426
Pham MT, Briançon L, Dias D, Abdelouhab A (2018a) Investigation of load transfer mechanisms in granular platforms reinforced by geosynthetics above cavities. Geotext Geomembr 46:611–624. https://doi.org/10.1016/j.geotexmem.2018.04.015
Pham VH, Dias D, Dudchenko A (2018b) 3D modeling of geosynthetic-reinforced pile-supported embankment under cyclic loading. Geosynth Int 27:157–169. https://doi.org/10.1680/jgein.18.00039
Pham MT, Vo DN, Nguyen DT, Do NA (2022) Numerical analysis of load transfer mechanisms within embankment reinforced by geosynthetic above cavity. Transp Infrastruct Geotech. https://doi.org/10.1007/s40515-021-00220-4
Pham MT (2019) Granular platform reinforced by geosynthetics above cavities-laboratory experiments and numerical modeling of load transfer mechanisms. PhD Dissertation, University of Grenoble Alpes, France.
PLAXIS (2020) PLAXIS 2-D Manuals. ISBN-13: 978-90-76016-20-7, Netherlands
Potts VJ, Zdravkovic L (2010) Finite-element study of arching behaviour in reinforced fills. Proc Institut Civil Eng Ground Improv 163:217–229
Rui R, Ye Y, Han J, Zhai Y, Wan Y, Chen C, Zhang L (2022) Two-dimensional soil arching evolution in geosynthetic-reinforced pile-supported embankments over voids. Geotext Geomembr 50(1):82–98. https://doi.org/10.1016/j.geotexmem.2021.09.003
Serridge CJ, Cooper AH (2023) Natural and anthropogenic halite karst subsidence in north Cheshire UK; comparison

of Rostherne Mere, Melchett Mere, Tatton Mere and their surroundings. Q J Eng Geol Hydrogeol. https://doi.org/10.1144/qjegh2022-081

Singh K, Dhar B (1997) Sinkhole subsidence due to mining. Geotech Geol Eng 15:327–341. https://doi.org/10.1023/A:1018471911108

Terzaghi K (1943) Theoretical soil mechanics. John Wiley Sons, Inc., New Jersey

Van Dyk C, Jacobsz SW (2016) The behaviour of a reinforced soil mattress spanning a cavity modelled in a geotechnical centrifuge. Geotech Geol Eng 34:1345–1358. https://doi.org/10.1007/s10706-016-0046-2

Villard P, Briançon L (2008) Design of geosynthetic reinforcements for platforms subjected to localized sinkholes. Can Geotech J 45:196–209. https://doi.org/10.1139/T07-083

Villard P, Gourc JP, Giraud H (2000) A geosynthetic reinforcement solution to prevent the formation of localized sinkholes. Can Geotech J 37:987–999. https://doi.org/10.1139/cgj-37-5-987

Villard P, Huckert A, Briançon L (2016) Load transfer mechanisms in geotextile-reinforced embankments overlying voids: numerical approach and design. Geotext Geomembr 44:381–395. https://doi.org/10.1016/j.geotexmem.2016.01.007

Vo DN, Pham MT, Le VA, To VN (2022) Load transfer acting in basal reinforced piled embankments: a numerical approach. Transp Infrastruct Geotech. https://doi.org/10.1007/s40515-022-00271-1

Wang MC, Feng YX, Jao M (1996) Stability of geosynthetic-reinforced soil above a cavity. Geotext Geomembr 14:95–109. https://doi.org/10.1016/0266-1144(96)84939-9

Wang ZL, Ma F (2007) A Simple Soil Model for Complex Loadings. In: Computational Mechanics. Springer, Berlin, Heidelberg. https://doi.org/10.1007/978-3-540-75999-7_90

Zhuang Y, Li S (2015) Three-dimensional finite element analysis of arching in a piled embankment under traffic loading. Arab J Geosci 8:7751–7762. https://doi.org/10.1007/s12517-014-1748-5